An idealized polyhedral model and geometric structure for silicon nanotubes

2009 J. Phys.: Condens. Matter 21 075301

(http://iopscience.iop.org/0953-8984/21/7/075301)

J. Phys.: Condens. Matter **21** (2009) 075301 (12pp) doi:10.1088/0953-8984/21/7/075301

An idealized polyhedral model and geometric structure for silicon nanotubes

Richard K F Lee, Barry J Cox and James M Hill

Nanomechanics Group, School of Mathematics and Applied Statistics, University of Wollongong, Wollongong, NSW 2522, Australia

E-mail: barryc@uow.edu.au

Received 8 August 2008, in final form 11 December 2008
Published 13 January 2009
Online at stacks.iop.org/JPhysCM/21/075301

Abstract

In this paper, we introduce an idealized model of silicon nanotubes comprising an exact polyhedral geometric structure for single-walled silicon nanotubes. The silicon nanotubes considered here are assumed to be formed by sp^3 hybridization and thus the nanotube lattice is assumed to comprise only squares or skew rhombi. Beginning with the three postulates that all bond lengths are equal, all adjacent bond angles are equal, and all atoms are equidistant from a common axis of symmetry, we derive exact formulae for the geometric parameters such as radii, bond angles and unit cell length. We present asymptotic expansions for these quantities to the first two orders of magnitude. Because of the faceted nature of the polyhedral model we may determine a perceived inner radius for the nanotube, from which an expression for the wall thickness emerges. We also describe the geometric properties of some ultra-small silicon nanotubes. Finally, the values of the diameters for the polyhedral model are compared with results obtained from molecular dynamics simulations and some limited numerical calculations are undertaken to confirm the meta-stability of the proposed structures.

(Some figures in this article are in colour only in the electronic version)

1. Introduction

There is considerable interest in using silicon material as nanostructures, such as nanowires and nanotubes. Following the discovery of carbon nanotubes [1] which has resulted in many theoretical and experimental investigations of their properties [2], many other materials have been explored as a possible material for nanotubes, such as WS_2, Bi_2S_3, ZnS, GaN, BN, AlN, InP, Eu_2O_3 and V_2O_3 [3]. Silicon is located in the same group of the periodic table as carbon and possesses four valence electrons. Silicon's chemical similarity to carbon is based on the law of periodicity and therefore silicon is often suggested as an alternative for carbon. It is also readily available as the second most abundant element in the earth's crust, comprising 25.7% of the earth's crust by mass [4].

While silicon and carbon are in the same group of the periodic table, silicon nanotubes have a different bond configuration to carbon nanotubes. Carbon nanotubes have a very stable structure formed from sp^2 hybridized bonds [2, 5], which leads to carbon nanotubes adopting a hexagonal structure. On the other hand, silicon prefers sp^3 bond formation and it is predicted that the four-coordinated atoms form a square lattice [2, 8, 9, 6, 7]. Recently, experiments report that silicon nanotubes have been synthesized by physical and chemical vapour deposition [10, 11] and molecular beam epitaxy [12] and large diameter silicon nanotubes are observed by transmission electron microscopy [10].

Many theoretical investigations into the structure of silicon nanotubes assume a conventional 'rolled-up' model [13, 18, 6, 7, 14, 4, 15–17]. There are also some studies which consider the silicon nanotube to comprise a flat regular hexagonal silicon sheet [18, 6, 7, 19, 14], while others begin with a puckered hexagonal silicon sheet [6, 7, 19, 4, 20], while still others start with a flat square silicon sheet [2, 8, 9, 6, 7].

Cox and Hill [23, 24] propose a new polyhedral model of single-walled carbon nanotubes that makes prediction of the geometric parameters of the tube which are in excellent agreement with first-principles calculations [23]. For the present work we employ a similar polyhedral model to represent single-walled silicon nanotubes. The silicon nanotubes considered here are all assumed to comprise a square lattice or a skew rhombic lattice of four-coordinated atoms. We comment that in proposing the new polyhedral model having all bond lengths equal, we have in mind a first

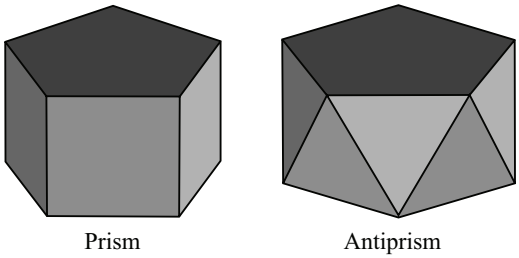

Figure 1. Pentagonal prism and antiprism.

level model, for which any subsequent modifications such as unequal bond lengths, can be incorporated later into the ideal model.

For the nanotubes considered here every silicon atom is assumed to be bonded to four others via sp^3 hybridized bonding. Hence, these silicon nanotubes can be considered to be constructed from either square or skew rhombus lattices [2, 8, 9, 6, 7]. Following the same concept of carbon nanotubes in the conventional 'rolled-up' model [15–17], silicon nanotubes can be conceptualized as a two-dimensional sheet of silicon with square lattice pattern, which is then rolled into a right circular cylinder. The terminology adopted for carbon nanotubes, namely zigzag and armchair, is entirely inappropriate for silicon nanotubes, and here we propose to categorize these tubes as being either prismatic, antiprismatic or chiral type based on the values of the chiral vector numbers (n, m). When $m = 0$, we find that the nanotube comprises a series of regular n-sided polygons, where the length of each polygon side and the height of the prism is simply equal to the bond length σ, and therefore we refer to these nanotube types as prismatic. In the case $m = n$, the nanotube comprises rows of atoms which are regular n-sided polygons with a rotation such that each vertex is located at the centre of the side of the preceding polygon but translated along the nanotubes axis. Thus, when each atom is joined to the two closest vertices of the preceding polygon, an antiprism is formed and therefore we term these nanotubes as antiprismatic. Figure 1 shows a pentagonal prism and antiprism. In all other cases, when $0 < m < n$, we follow the carbon nanotube terminology and term the nanotube chiral.

The polyhedral model for the silicon nanotubes is developed in the same manner as that for carbon nanotubes [23, 24] and is based on three fundamental postulates: (i) all bond lengths are equal σ; (ii) all the adjacent bond angles are equal ϕ; and (iii) all atomic nuclei are equidistant from a common axis r. The silicon nanotubes represented with the polyhedral model are shown in figure 2. In this figure the silicon atoms are represented by black dots and the bonds between silicon atoms are indicated by black lines, all of which are the same length based on postulate (i).

In section 2 we introduce the polyhedral model for silicon nanotubes and the derivations for the major equations of the polyhedral model. In section 3, we give the asymptotic expansions for these formulae for the first two leading terms. In section 4, we explore the geometric structure of some ultra-small nanotubes and in section 5, we compare our results

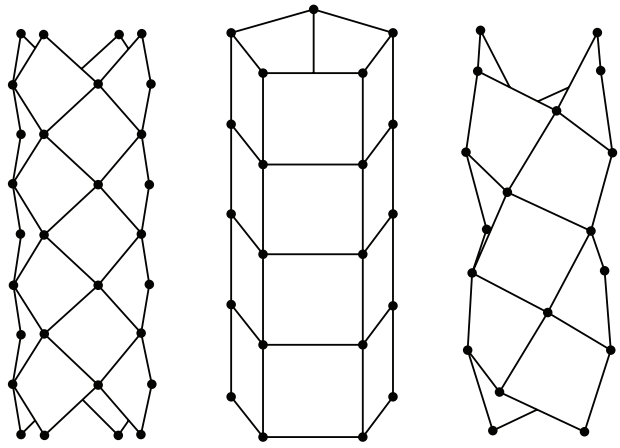

Figure 2. Silicon nanotubes for the polyhedral model for antiprismatic, prismatic and chiral type.

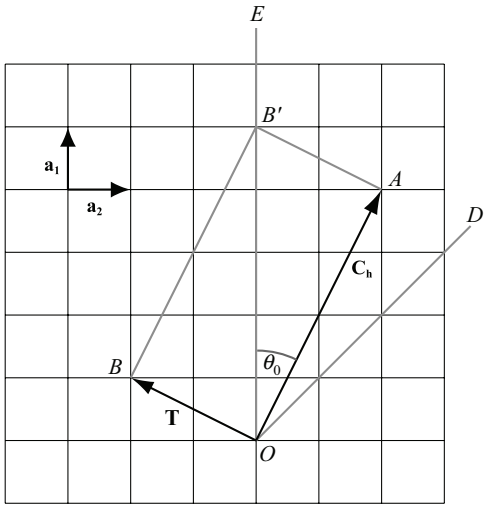

Figure 3. Silicon nanotube constructed from two-dimensional sheet.

for these and demonstrate a good agreement with molecular dynamics method and we describe the general behaviour of the major geometric parameters. Some concluding remarks are made in section 6 and finally the details of the asymptotic expansions are presented in appendix.

2. The polyhedral model for silicon nanotubes

Employing the same concept as that used for carbon nanotubes, we apply the (n, m) naming scheme to identify the specific configuration of the silicon nanotube originating from a 'rolled-up' model [15–17]. In this model, the silicon nanotubes are conceptualized as a flat plane of four-coordinated silicon atoms which is then rolled into a right circular cylinder. From figure 3, three different types of silicon nanotubes can be defined by the value of m in relation to n. The naming convention we employ for silicon nanotubes is different to the corresponding convention adopted for hexagonal latices, e.g. carbon nanotubes. This difference is necessary because the

conventional terms are not applicable to the silicon geometry. When $m = 0$, we term the resulting nanotube to be the prismatic type. This is equivalent to the direction of rolling up of the nanotube OE and we use this term because the tube comprises regular n-gon prisms. The second type, which we term the antiprismatic type, occurs when $m = n$. In this case, the sheet is rolled following the direction OD.

The chiral type is a direction which is between OD and OE. The (n, m) naming scheme of the nanotube can be thought of as the chiral vector $\mathbf{C_h}$, shown on figure 3. In this figure we show a silicon nanotube of type (4, 2). The vector OB is called the unit translational vector $\mathbf{T}$ and consists of the coefficients of $\mathbf{a_1}$ and $\mathbf{a_2}$ to be divided by the greatest common divisor d_R of n and m. Therefore we have

$$\mathbf{C_h} = n\mathbf{a_1} + m\mathbf{a_2},$$

$$\mathbf{T} = -m\mathbf{a_1}/d_R + n\mathbf{a_2}/d_R,$$

where n and m are the integers from the (n, m) naming scheme, $\mathbf{a_1}$ and $\mathbf{a_2}$ are the unit vectors in real space, and d_R is the greatest common divisor of n and m.

In figure 3 the origin O is located at an arbitrary lattice point. The chiral vector $\mathbf{C_h}$ goes from O to A. The vector between O and B is called a translational vector $\mathbf{T}$. The sheet is rolled up to form a nanotube where the point A will coincide with the origin O and the point B will coincide with the point B′. From figure 3 the conventional chiral angle θ_0 is found to be

$$\cos^2\theta_0 = n^2/(n^2 + m^2). \tag{1}$$

The unit cell length L_0 for the 'rolled-up' model is the length of the translational vector $|\mathbf{T}|$, which is given by

$$L_0 = \sigma\sqrt{n^2 + m^2}/d_R. \tag{2}$$

The conventional radius equation for the nanotube is obtained from a simple geometric method, and is given by the magnitude of the chiral vector $|\mathbf{C_h}|$, divided by 2π and thus

$$r_0 = \sigma\sqrt{n^2 + m^2}/2\pi. \tag{3}$$

The polyhedral model for silicon nanotubes is similar to the equivalent carbon nanotube model [23, 24]. From the fundamental postulate (iii), all atoms in the silicon nanotube are equidistant from a common axis, and thus the vertices of each face cannot be coplanar and therefore in the rolled-up state, the lattice comprises skew rhombi. For the carbon nanotubes, a hexagonal lattice is divided into three isosceles triangles and one equilateral triangle [23, 24]. However, as we demonstrate below, we do not need to subdivide the skew rhombic lattice.

We begin by defining a cylinder which is traced by helices that correspond to the lattice lines in the direction of $\mathbf{a_1}$. Therefore, from figure 3 it may easily be shown that the number of helices is equivalent to the value of m and the silicon atoms are positioned on these helices. Therefore, the first helix $\alpha(t)$ on the cylinder has the parametric form in Cartesian coordinates

$$\alpha(t) = (r\cos(2\psi t/m), r\sin(2\psi t/m), bt/m), \tag{4}$$

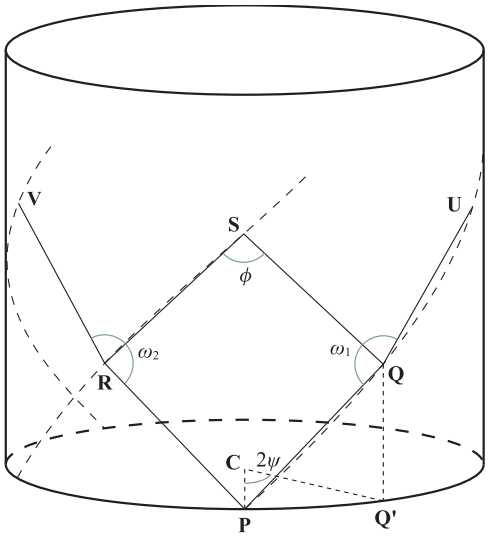

Figure 4. Points lying on three helices and forming an equilateral skew rhombus in three-dimensional space.

where 2ψ is the angle subtended at the nanotube axis in the xy-plane of one edge of a skew rhombus, r is the radius of the nanotube, b is the helical vertical spacing coefficient and t is a parametric variable which has been chosen such that the vertices are spaced evenly at a distance m in this variable.

The Cartesian coordinates of points **P**, **Q** and **U** in figure 4 are found from (4). The point $\mathbf{P} = \alpha(0) = (r, 0, 0)$ in Cartesian coordinates, the point $\mathbf{Q} = \alpha(m) = (r\cos 2\psi, r\sin 2\psi, b)$ and the point $\mathbf{U} = \alpha(2m) = (r\cos 4\psi, r\sin 4\psi, 2b)$. Therefore the distance of the bond σ, which is between the point **P** and the point **Q**, in three-dimensional space is given by $\sigma^2 = 4r^2\sin^2\psi + b^2$.

Similarly, the second helix $\beta(t)$ is congruent to the first but rotated through an angle of $2\pi/m$. The parametric equation is given by

$$\beta(t) = (r\cos[2(\psi t - \pi)/m], r\sin[2(\psi t - \pi)/m], bt/m). \tag{5}$$

Furthermore, the third helix $\gamma(t)$ is symmetric to the second with its coordinates rotated through a further $2\pi/m$ in the angular dimension. Thus the parametric equation is given by

$$\gamma(t) = (r\cos[2(\psi t - 2\pi)/m], r\sin[2(\psi t - 2\pi)/m], bt/m). \tag{6}$$

In figure 4, the two points **R** and **S** are found from (5) and the point **V** is found from (6). The point $\mathbf{R} = \beta(n)$, the point $\mathbf{S} = \beta(n + m)$ and the point $\mathbf{V} = \gamma(2n)$. The four points of **P**, **Q**, **R** and **S** comprise a skew rhombus. From postulate (i) we require all edges of the rhombus to be equal, and therefore $|\mathbf{PQ}| = |\mathbf{RS}| = |\mathbf{PR}| = |\mathbf{QS}| = \sigma$. This postulate then gives rise to the following expressions

$$|\mathbf{PQ}|^2 = |\mathbf{RS}|^2 = 4r^2\sin^2\psi + b^2,$$

$$|\mathbf{PR}|^2 = |\mathbf{QS}|^2 = 4r^2\sin^2\xi + (nb/m)^2,$$

where $\xi = (n\psi - \pi)/m$ and from postulate (i) we require $|\mathbf{PQ}| = |\mathbf{PR}|$ and therefore we may derive

$$b^2/r^2 = 4m^2\left(\sin^2\psi - \sin^2\xi\right)/(n^2 - m^2). \tag{7}$$

We also require the distances of $|\mathbf{QR}|$ and $|\mathbf{PS}|$ which are given by

$$|\mathbf{QR}|^2 = 4r^2\sin^2(\xi - \psi) + [(n-m)b/m]^2,$$

$$|\mathbf{PS}|^2 = 4r^2\sin^2(\xi + \psi) + [(n+m)b/m]^2.$$

From postulate (ii), we require the angle between adjacent bonds to be equal which is equivalent to the requirement that $|\mathbf{QR}| = |\mathbf{PS}|$. From this requirement we may derive

$$b^2/r^2 = (-4m\sin\xi\cos\xi\sin\psi\cos\psi)/n. \tag{8}$$

As a result, the two equations (7) and (8) are employed to derive an equation for the fundamental parameter, the subtend semi-angle ψ, given by

$$n\tan\xi + m\tan\psi = 0, \tag{9}$$

where $\xi = (n\psi - \pi)/m$. The subtend semi-angle ψ, is determined as the root of this equation. Equation (9) may have many roots, but based on a specific requirement that the subtend semi-angle ψ, must also satisfy the inequalities (10), since $\xi \leqslant 0 \leqslant (\xi + \psi)$, we obtain the following inequalities:

$$\pi/(n+m) \leqslant \psi \leqslant \pi/n. \tag{10}$$

The root of (9) which also satisfies (10) can be accurately determined numerically by a small number of iterations of Newton's method, using the initial value of the root given by $\psi_0 = n\pi/(n^2 + m^2)$. From (9) the exact values of the subtend semi-angle ψ are found as $\psi = \pi/2n$ for the antiprismatic type $m = n$ and $\psi = \pi/n$ for the prismatic type $m = 0$.

The true chiral angle θ, is found by considering a triangle comprising the points **P**, **Q** and **Q**′ which is the point determined by projecting **Q** into the xy-plane as shown in the figure 5. Therefore, the distance c^2 is given by

$$c^2 = 4r^2(n^2\sin^2\psi - m^2\sin^2\xi)/(n^2 - m^2).$$

From figure 5 the distance d is deduced by the cosine law, given by

$$d = 2r\sin\psi, \tag{11}$$

and b^2 is given by (7). One result of this derivation is that the true chiral angle θ can be expressed by

$$\cos^2\theta = \frac{n^2\cos^2\psi + m^2\sin^2\psi}{n^2\cos^2\psi + m^2}. \tag{12}$$

In view of the fact that we have two expressions for b^2 in (7) and (8), the true chiral angle θ can also be expressed in the same form given in (12), where c^2 is given by

$$c^2 = 4r^2\sin^2\psi[1 - (m/n)\sin\xi\cos\xi\cot\psi].$$

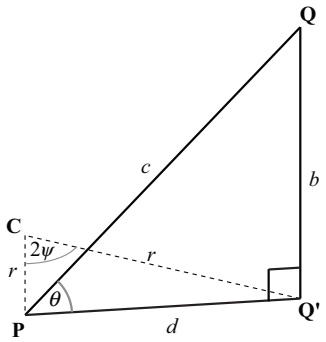

Figure 5. Points forming **PQQ**′ in three-dimensional space.

The adjacent bond angle ϕ is defined as the angle between two bonds where the atoms that are being bonded comprise a single square or a single skew rhombus in the nanotube lattice and the opposite bond angles are the angle between two bonds where the atoms that are being bonded comprise different squares or skew rhombi in the nanotube lattice. The adjacent bond angle ϕ and the two opposite bond angles ω_1 and ω_2 are derived from the cosine law. The adjacent bond angle is found by considering a triangle comprising the points **R**, **S** and **Q**. Using the same technique, the opposite bond angle ω_1 is found from the triangle Δ**PQU** and the opposite bond angle ω_2 is found from the triangle Δ**PRV**. The adjacent bond angle ϕ is given by

$$\cos\phi = (m^2\sin^2\psi)/(n^2\cos^2\psi + m^2), \tag{13}$$

and the opposite bond angles ω_1 and ω_2 are given by

$$\cos\omega_1 = 2\cos^2\theta\sin^2\psi - 1, \tag{14}$$

$$\cos\omega_2 = \frac{2(m^2 - n^2\tan^2\theta)}{m^2 + n^2\cos^2\psi} - 1. \tag{15}$$

The nanotube radius r is the distance from the silicon atoms to the axis of the nanotube which may be found from $\cos\theta$ in figure 5 and the length of $|\mathbf{PQ}| = \sigma = c$, the length of the silicon–silicon covalent bond. The value of d may be obtained from (11) and $\cos\theta = d/c$. We may also envisage an inner radius r_{in} as the closest perpendicular distance of all bonds, which is the midpoint of the closest silicon–silicon bond, and the nanotube axis. The nanotube radius r and the perceived inner radius are found to be given by

$$r = (\sigma\cos\theta)/(2\sin\psi), \qquad r_{\text{in}} = r\cos\psi, \tag{16}$$

where σ is the length of the silicon–silicon bond.

As a consequence of the polyhedral model, silicon nanotubes can be viewed as having a wall thickness arising from the two radii, such that the hollow cylinder of radii r and r_{in} is precisely the smallest such cylinder which can enclose all atoms and bonds of the nanotube. The nanotube thickness δ is defined as the difference between these two radii and is given by

$$\delta = [\sigma\cos\theta\tan(\psi/2)]/2. \tag{17}$$

Silicon nanotubes are also considered to be constructed from a repeating unit cell. The number of atoms in a unit cell,

a rectangle of OAB′B, in figure 3 is the number of atoms N in the unit cell which is given by $N = |\mathbf{C_h} \times \mathbf{T}|/|\mathbf{a_1} \times \mathbf{a_2}|$. Thus the number of atoms in the unit cell for the polyhedral model is found as

$$N = (n^2 + m^2)/d_R,$$

where d_R is the greatest common divisor of n and m. A unit cell length L is the number of atoms in a single helix multiplied by the helical vertical spacing coefficient b. The number of atoms in a single helix is found from the number of atoms in a unit cell N divided by m helices. Thus for the unit cell length may be derive from $L = Nb/m$ and is given by

$$L = [\sigma(n^2 + m^2)\sin\theta]/(md_R). \tag{18}$$

3. Asymptotic expansions for the polyhedral model

As shown in appendix the equations of the polyhedral model may be expressed in terms of expansions of n and m in the limit of $n \to \infty$ by using the method of asymptotic expansions. The subtend semi-angle ψ determined from the transcendental equation (9) is given by

$$\psi = \frac{n\pi}{n^2 + m^2} - \frac{nm^2\pi^3(n^2 - m^2)}{3(n^2 + m^2)^4} + \mathrm{O}\left(\frac{1}{n^5}\right), \tag{19}$$

where the $\mathrm{O}(1/n^5)$ term refers to the maximum order of the magnitude of the next most significant term. The first term of (19) gives the leading order behaviour for the subtend semi-angle ψ and the second term is a correction term which takes into account the curvature of the cylinder in question. The subtend semi-angle ψ can be rewritten a series using the Lagrange expansion which is given by

$$\psi = \sum_{k=0}^{\infty} \frac{1}{(2k+1)!} \times \left[\frac{\mathrm{d}^{2k}}{\mathrm{d}\Psi^{2k}}\left(\frac{\pi\Psi}{n\Psi + m\tan^{-1}(\frac{m}{n}\tan\Psi)}\right)^{2k+1}\right]_{\Psi=0}. \tag{20}$$

It is worth commenting that up to this order (19) and (20) are totally in accordance with the special cases of antiprismatic nanotubes $n = m$, where $\psi = \pi/2n$, as well as the case of prismatic nanotubes $m = 0$, where $\psi = \pi/n$.

By substituting (19) into the expressions for the chiral angle θ given in (12) and then by further expansion in terms of $1/n$, an expansion for the chiral angle θ may be developed which is given by

$$\cos^2\theta = \frac{n^2}{n^2 + m^2} + \frac{n^2m^4\pi^2}{(n^2 + m^2)^4} + \mathrm{O}\left(\frac{1}{n^4}\right), \tag{21}$$

where the leading order term is exactly the conventional expression (1). The second term is the first-order correction to the conventional chiral angle θ_0 and it may be shown that (21) can be expressed as

$$\cos^2\theta = \cos^2\theta_0 + \frac{\sigma^2\cos^2\theta_0\sin^4\theta_0}{4r_0^2} + \mathrm{O}\left(\frac{1}{n^4}\right). \tag{22}$$

The expansion equation for the adjacent bond angle ϕ is found by substituting (19) in equation (13), where upon the expansion of $\cos\phi$ is given by

$$\cos\phi = \frac{n^2m^2\pi^2}{(n^2 + m^2)^3} + \frac{n^2m^2\pi^4(2n^4 - 3n^2m^2 + 2m^4)}{3(n^2 + m^2)^6} + \mathrm{O}(1/n^6).$$

The two opposite bond angles, ω_1 and ω_2 are expanded by substituting (19) and (21) into the equations (14) and (15) for $\cos\omega_1$ and $\cos\omega_2$ to obtain

$$\cos\omega_1 = -1 + \frac{2n^4\pi^2}{(n^2 + m^2)^3} - \frac{2n^4\pi^4(n^4 + 3n^2m^2 - 5m^4)}{3(n^2 + m^2)^6} + \mathrm{O}(1/n^6),$$

$$\cos\omega_2 = -1 + \frac{2m^4\pi^2}{(n^2 + m^2)^3} - \frac{2m^4\pi^4(m^4 + 3n^2m^2 - 5n^4)}{3(n^2 + m^2)^6} + \mathrm{O}(1/n^6).$$

Using the same technique asymptotic expansions may be developed for the nanotube outer radius r, the thickness δ and the unit cell length L. The nanotube radius r is given by

$$r = \frac{\sigma\sqrt{n^2 + m^2}}{2\pi} + \frac{\pi\sigma(n^4 + 3n^2m^2 + m^4)}{12(n^2 + m^2)^{5/2}} + \mathrm{O}\left(\frac{1}{n^3}\right), \tag{23}$$

where the leading order term is exactly the conventional expression (3). Similarly, it can be shown that the second term is a first-order correction to the conventional radius which is due to the curvature of the structure, which can be written in terms of the conventional chiral angle θ_0 and the conventional radius r_0 by (1) and (3) as

$$r = r_0 + \frac{\sigma^2}{192r_0}[9 - \cos(4\theta_0)] + \mathrm{O}\left(\frac{1}{n^3}\right). \tag{24}$$

The thickness δ is given by the expansion

$$\delta = \frac{n^2\pi\sigma}{4(n^2 + m^2)^{3/2}} + \frac{n^2\pi^3\sigma(n^4 - 3n^2m^2 + 10m^4)}{48(n^2 + m^2)^{9/2}} + \mathrm{O}(1/n^5). \tag{25}$$

Both terms in (25) are new since there is at present no theory on silicon nanotube thickness. The order of the leading term is $1/n$ and thus the thickness tends to approach zero as the size of the nanotube increases. This is expected since the thickness is a measure of the curvature of the faceted surface model. We also note that the thickness can be approximated by the relation

$$\delta = (\sigma^2\cos^2\theta_0)/(8r_0) + \mathrm{O}(1/n^3).$$

An asymptotic expansion of the unit cell length L yields

$$L = \frac{\sigma\sqrt{n^2 + m^2}}{d_R} - \frac{n^2m^2\pi^2\sigma}{2(n^2 + m^2)^{5/2}d_R} + \mathrm{O}\left(\frac{1}{n^3}\right), \tag{26}$$

where we note that the first term in (26) is exactly the conventional expression (2). It may be shown that the second term is a first-order correction to the conventional unit cell length which is due to the curvature of the structure, which is given by

$$L = L_0 - \frac{\pi\sigma^2}{32r_0d_R}[1 - \cos(4\theta_0)] + \mathrm{O}\left(\frac{1}{n^3}\right). \tag{27}$$

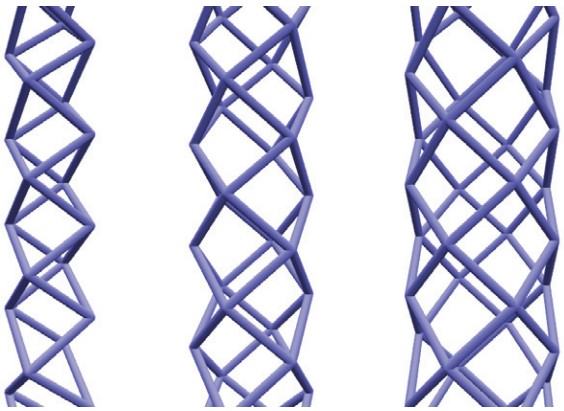

Figure 6. (2, 2), (3, 3), (4, 4) antiprismatic silicon nanotubes.

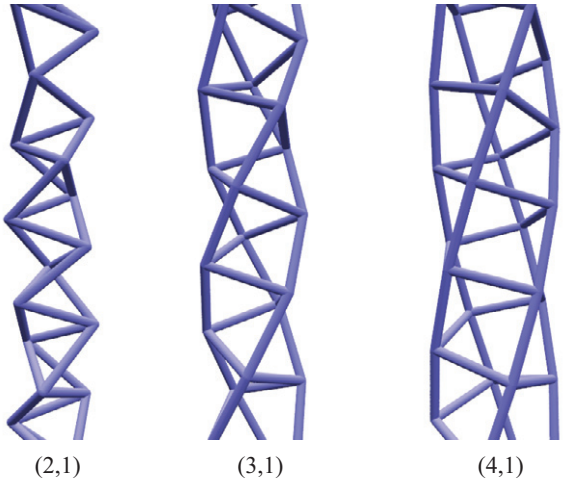

Figure 7. (2, 1), (3, 1), (4, 1) chiral silicon nanotubes.

4. Geometric structure of ultra-small silicon nanotubes

In this section we consider the structure of silicon nanotubes, as described by the polyhedral model, in the limit of decreasing radius. We shall see that in some cases polyhedral geometric structures arise, while in other cases, the nanotubes cannot be constructed at all. The ultra-small silicon nanotubes considered here are those shown in figures 6–8. We comment however, that the large deviations in bond angles would make these structures very difficult to realize in practice.

Antiprismatic silicon nanotubes of types (2, 2), (3, 3) and (4, 4) are shown in figure 6. The (4, 4) silicon nanotube appears as a reasonably tubular structure, but the (3, 3) tube is between a cylindrical structure and a polyhedral structure due to the increased curvature. The (2, 2) silicon nanotube shows a highly nontubular polyhedral structure to accommodate the inherent large curvature. The (1, 1) silicon nanotube does not arise because the value of b from (8) is zero and the tube becomes a single bond of silicon where all atoms coincide with each other and as a result it is not within the scope of the model presented here.

In figure 7 we show some chiral nanotubes of type (2, 1), (3, 1) and (4, 1). We comment that the (2, 1) tube has a highly nontubular polyhedral structure to accommodate the high curvature of the surface. These two figures demonstrate that the structure of the antiprismatic and the chiral tubes is dependent on the tube radius.

Prismatic silicon nanotubes are shown in figure 8. As expected the (4, 0) has a square tube shape and the (3, 0) has a triangular structure. The (2, 0) is ladder-like but since in our model all the silicon nanotubes are assumed to comprise four-coordinated atoms, the present model does not apply for (2, 0) tubes. The (1, 0) tube does not arise because the value of the nanotube radius r is divided by zero, since the subtend semi-angle is 180°, so again it is not within the scope of the present model. Ultra-small silicon nanotubes tend not to be produced in experiments due to their highly faceted structure. Also very large nanotubes do not occur in experiments and therefore the radii of nanotubes tends to lie in a definite range.

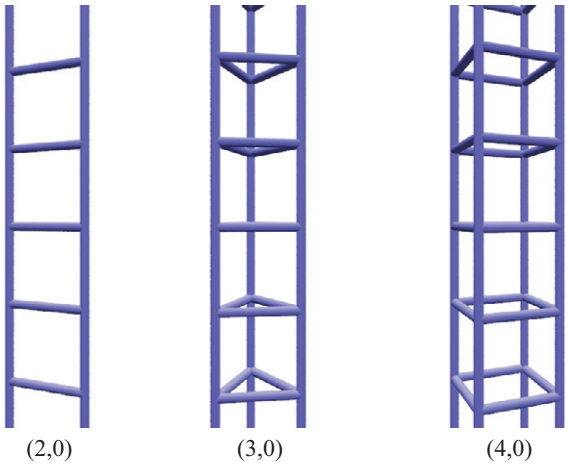

Figure 8. (2, 0), (3, 0), (4, 0) prismatic silicon nanotubes.

5. Results

Various authors have reported different values for the silicon–silicon bond length for nanotubes. For example, based on the Tersoff potential, the silicon bond length is found to be 2.305 Å [13, 25, 14, 26]. For the formation of the sp^3 hybridization, the single silicon–silicon bond length is 2.35 Å [5, 28, 27]. Other values that have been reported are 2.34, 2.36 and 2.38 Å, which also come from the formation of the sp^3 hybridization [29, 32, 30, 26, 31, 6]. These variations in bond length may in part be due to the deficiencies in the various simulation approximations or to the authors adopting the bond length from silicon structures other than nanotubes.

The nanotube type (n, m), subtend angle 2ψ, true chiral angle θ, adjacent bond angle ϕ, opposite bond angles ω_1 and ω_2, nanotube radius r, unit cell length L and thickness δ for a variety of nanotubes for $2 \leqslant n \leqslant 5$ are shown in table 1, where we have assumed a silicon–silicon bond length of $\sigma = 2.35$ Å.

We now compare our results with the molecular dynamics studies of Li *et al* [2] who examine a number of prismatic silicon nanotubes using an empirical full-potential linear-muffin-tin-orbital molecular dynamics method. Their silicon

Table 1. Results of the polyhedral model using $\sigma = 2.35$ Å.

(n, m)	2ψ (deg)	θ (deg)	ϕ (deg)	ω_1 (deg)	ω_2 (deg)	r (Å)	L (Å)	δ (Å)
(2, 1)	131.81	18.43	60.00	60.00	109.47	1.221	3.716	0.723
(2, 2)	90.00	35.26	70.53	109.47	109.47	1.357	2.714	0.397
(3, 0)	120.00	0.00	90.00	60.00	180.00	1.357	2.350	0.678
(3, 1)	104.48	17.02	81.79	81.79	158.21	1.421	6.880	0.551
(3, 2)	80.66	30.12	79.54	111.92	142.16	1.570	7.666	0.373
(3, 3)	60.00	40.89	81.79	135.58	135.58	1.776	3.077	0.238
(4, 0)	90.00	0.00	90.00	90.00	180.00	1.662	2.350	0.487
(4, 1)	83.69	13.71	87.42	99.20	172.03	1.711	9.469	0.436
(4, 2)	70.53	25.24	84.78	117.04	159.95	1.841	5.010	0.338
(4, 3)	56.86	34.80	84.52	133.98	151.74	2.027	11.175	0.244
(4, 4)	45.00	42.73	85.47	147.35	147.35	2.255	3.189	0.172
(5, 0)	72.00	0.00	90.00	108.00	180.00	1.999	2.350	0.382
(5, 1)	68.88	11.21	88.98	112.62	176.33	2.038	11.876	0.357
(5, 2)	61.33	21.27	87.35	123.25	168.83	2.147	12.359	0.300
(5, 3)	52.30	29.92	86.56	135.09	161.93	2.311	13.285	0.237
(5, 4)	43.61	37.30	86.63	145.63	157.05	2.516	14.598	0.180
(5, 5)	36.00	43.56	87.13	154.12	154.12	2.755	3.239	0.135

Table 2. Comparison of silicon nanotube diameters from the conventional model, the polyhedral model and the molecular dynamics method of Li *et al* [2] using $\sigma = 2.305$ Å.

(n, m)	$2r_0$ (Å)	$2r$ (Å)	Li *et al* [2] (Å)
(6, 0)	4.402	4.610	4.7
(8, 0)	5.870	6.023	6.0
(10, 0)	7.337	7.459	7.5

nanorings and nanotubes are prismatic silicon nanotubes with atoms at the surface, and their nanotubes are similar to the prismatic nanotubes described here. Table 2 shows a comparison of diameters using the bond length $\sigma = 2.305$ Å. This table shows that the results of the polyhedral model are in excellent agreement with those of the molecular dynamics study.

Apart from the contribution of Li *et al* [2], there appears to be no literature on four-coordinated silicon nanotubes either experimentally or in molecular dynamics simulations. To provide some confidence that the structures considered here are at least meta-stable, we relaxed the idealized nanotube structures using the LAMMPS software (see Plimpton [21]) and we model the silicon pairwise interactions using a Stillinger–Weber potential [22]. Our approach is then to establish the simulation for an initial temperature of 600 K which we reduce to 0 K over 100 000 time steps, and at the end of the simulation the structures are examined for inconsistencies. For prismatic tubes $(n, 0)$ with $n \in \{5, 6, \ldots, 10\}$, the simulation domain extends 6 nm in the x and y directions and 5.12 nm in the z direction, which is the direction the nanotube axis is aligned and we also employ a periodic boundary condition in this direction. This provides enough space to include 20 rings of n atoms which are then assumed to repeat into what is essentially an infinite silicon nanotube. The results of these simulations are that for $n = 5$, 6 or 7, the initial pairwise energies are in the range -3.321 to -3.413 eV/atom and the corresponding relaxed pairwise energies are in the range -3.340 to -3.429 eV/atom. This shows that there is little change in these structures during the relaxation process, which agrees with a visual inspection of the relaxed structure and supports the hypothesis that these structures are meta-stable. However, for $n = 8$, 9 and 10, the initial pairwise energies are in the range -3.164 to -3.260 eV/atom but the corresponding relaxed pairwise energies in these cases are significantly lower, being in the range -3.567 to -3.578 eV/atom. This indicates that silicon nanotubes of this size are not stable under these conditions and a visual inspection shows significant changes in structure. It is not the intention of this investigation to perform a detailed structural study of silicon nanotubes but rather to provide some indication that the structures may be meta-stable. These calculations suggest that there is some evidence for meta-stability, especially for smaller prismatic silicon nanotubes. For purposes of comparison, we note that using the same potential function Stillinger and Weber [22] report a pairwise energy of -4.334 eV/atom for diamond cubic silicon at 0 K, which is the energetically preferred structure for silicon at this temperature.

Figure 9 shows a plot of the subtend angle 2ψ against n and shows that the subtend angle increases as the value of n decreases. This phenomenon is due to the curvature of the tube surface increasing as n decreases, so that the nanotubes with the smallest values of n have the largest curvature. The value of the chiral angle for zigzag carbon nanotubes is constant at zero, independent of n, both in the conventional model and also in the polyhedral model [23]. Similarly, the chiral angle value for prismatic silicon nanotubes is also zero. On the other hand, the chiral angle value for armchair carbon nanotubes is 30°, which is also independent of n, for both models [23]. However, for the case of antiprismatic silicon nanotubes, the chiral angle depends on n. For the conventional model, the value of the chiral angle is a constant, 45°. Figure 10 shows that the chiral angle starts from 35.26° and asymptotes to 45° in the limit as n becomes large.

Figure 11 shows that the value of the adjacent bond angle ϕ for the prismatic type is independent of n and the value is a constant, 90°. The value of the adjacent bond angle for the chiral and the antiprismatic types asymptotes to 90° in the

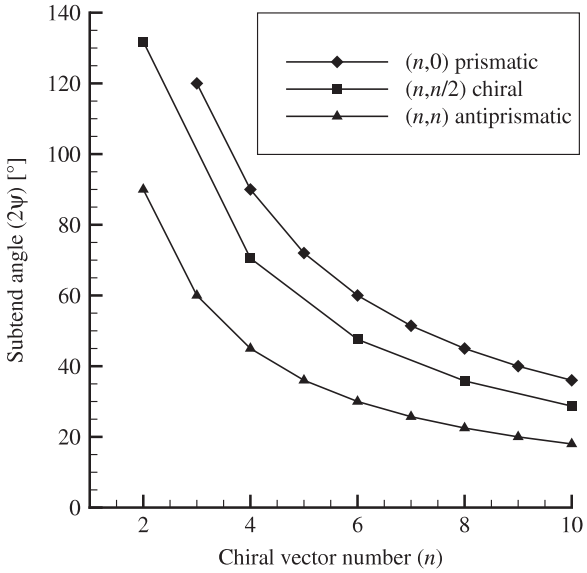

Figure 9. Subtend angle 2ψ for silicon nanotubes of type prismatic: (3, 0)–(10, 0), chiral: (2, 1)–(10, 5) and antiprismatic: (2, 2)–(10, 10).

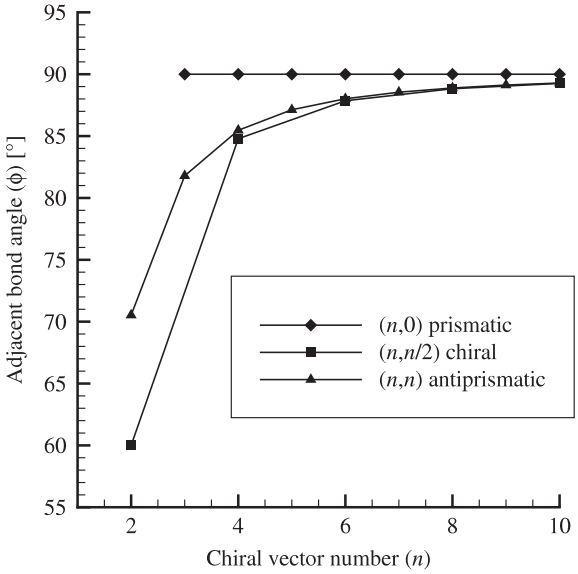

Figure 11. Adjacent bond angle ϕ for silicon nanotubes of type prismatic: (3, 0)–(10, 0), chiral: (2, 1)–(10, 5) and antiprismatic: (2, 2)–(10, 10).

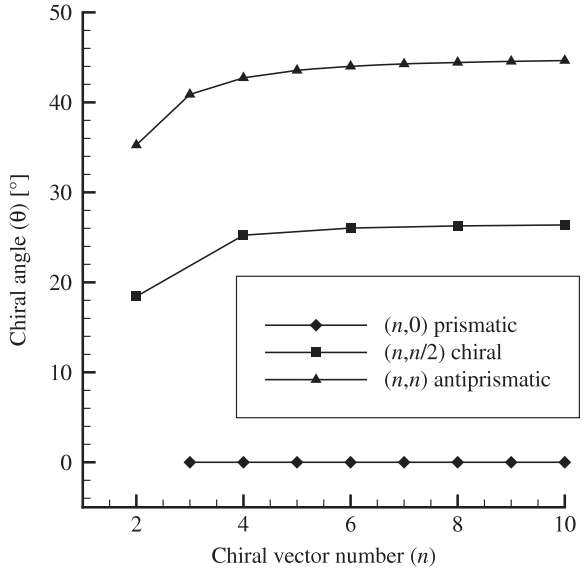

Figure 10. Chiral angle θ for silicon nanotubes of type prismatic: (3, 0)–(10, 0), chiral: (2, 1)–(10, 5) and antiprismatic: (2, 2)–(10, 10).

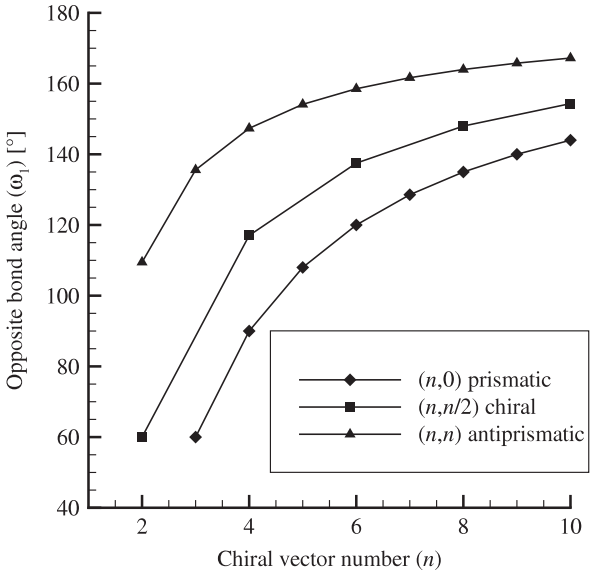

Figure 12. Opposite bond angle ω_1 for silicon nanotubes of type prismatic: (3, 0)–(10, 0), chiral: (2, 1)–(10, 5) and antiprismatic: (2, 2)–(10, 10).

limit as n becomes large, since the surface of the nanotube approaches a flat plane in this limit. The values of the opposite bond angle ω_1 for all three types asymptote to 180° in the limit as n becomes large, which is shown in figure 12. Similarly, figure 13 shows that the value of the opposite bond angle ω_2 for the chiral and the antiprismatic types asymptote to 180°. The value of the opposite bond angles for the prismatic type is independent of n, which is a constant, 180°. The values of the opposite bond angles ω_1 and ω_2 are equal in the antiprismatic type. However, the large deviations of the Si–Si bond angles from the ideal tetrahedral angles indicate that these structures would be very challenging to synthesis.

Figure 14 shows the percentage difference between the polyhedral radius and the radius of the conventional ($r - r_0$)/r_0 × 100% as a function of n. We comment that as n decreases, this percentage difference in radii increases, due to the curvature of the nanotube which is not accommodated by the conventional model. On the other hand, the polyhedral model incorporates curvature and therefore the difference between the two models becomes most significant for small radius tubes. As n becomes large, the curvature becomes insignificant and the two models approach the same value for the radius. For example, when the value of n is greater than or equal to 6, the difference between the polyhedral model and the conventional model of radii is less then 5%, which includes two standard deviations. The percentage difference between

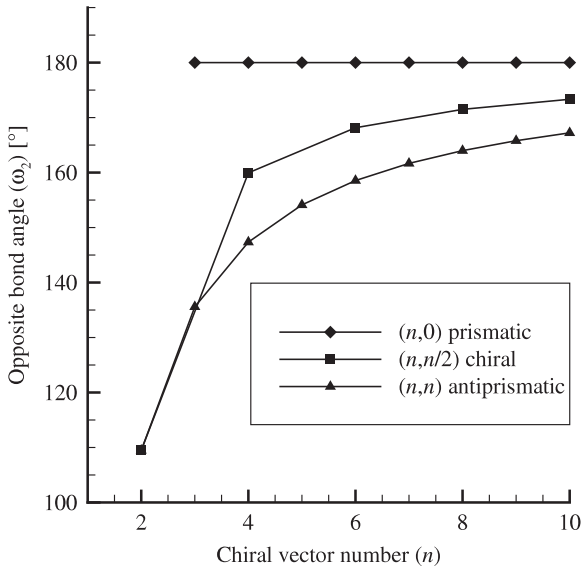

Figure 13. Opposite bond angle ω_2 for silicon nanotubes of type prismatic: (3, 0)–(10, 0), chiral: (2, 1)–(10, 5) and antiprismatic: (2, 2)–(10, 10).

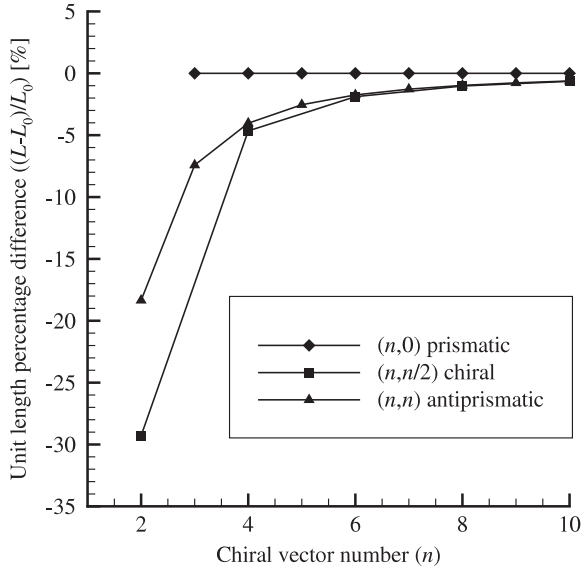

Figure 15. Percentage difference between the polyhedral model and conventional unit cell length $((L - L_0)/L_0)$ (%) for silicon nanotubes of type prismatic: (3, 0)–(10, 0), chiral: (2, 1)–(10, 5) and antiprismatic: (2, 2)–(10, 10).

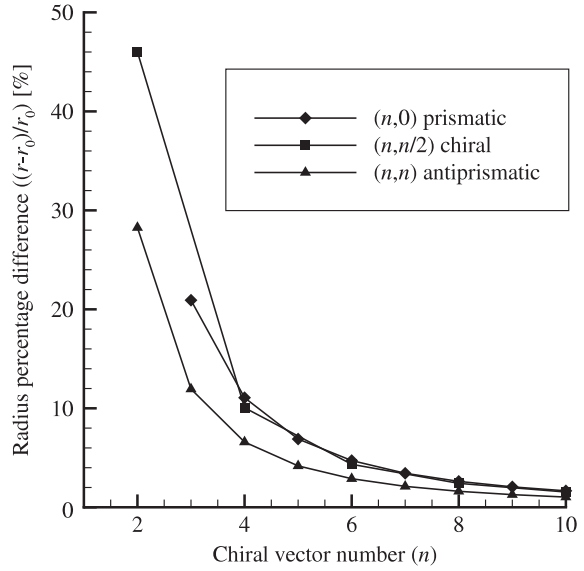

Figure 14. Percentage difference between the polyhedral model and conventional radius $((r - r_0)/r_0)$ (%) for silicon nanotubes of type prismatic: (3, 0)–(10, 0), chiral: (2, 1)–(10, 5) and antiprismatic: (2, 2)–(10, 10).

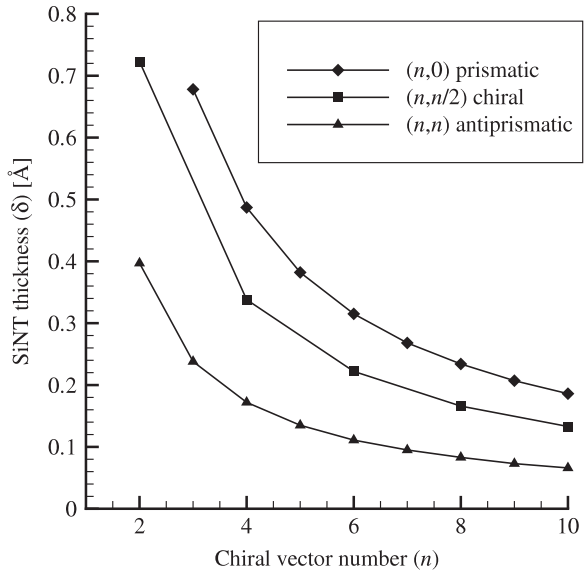

Figure 16. Thickness δ for silicon nanotubes of type prismatic: (3, 0)–(10, 0), chiral: (2, 1)–(10, 5) and antiprismatic: (2, 2)–(10, 10).

the two models for the radii is less than 2%, when the value of n is greater than or equal to 10.

Figure 15 shows the percentage difference between the unit cell length of the conventional model and the polyhedral model $(L - L_0)/L_0 \times 100\%$. For prismatic nanotubes there is no difference between the two models. However, for antiprismatic nanotubes there is a large difference as n decreases, and the percentage difference is negative, indicating that the unit cell length L is shorter than that of the conventional unit cell length L_0. The difference for chiral nanotubes increases from the prismatic value to a maximum value and then decreases to the antiprismatic value. We find that the maximum value of the unit cell length L for the chiral nanotubes occurs for either $(n, \lfloor n/\sqrt{2} \rfloor)$ or $(n, \lceil n/\sqrt{2} \rceil)$, where the floor symbols $\lfloor x \rfloor$ denote the greatest integer less than or equal to x, and the ceiling symbols $\lceil x \rceil$ denote the smallest integer greater than or equal to x.

A plot of the nanotube thickness versus n is shown in figure 16 for silicon nanotubes and figure 17 for carbon nanotubes in the polyhedral model, and we note that the two plots are very similar. For n small, the nanotube thickness becomes large, while for n large the thickness approaches zero. By examining the asymptotic expansions of the equations for

Table 3. Main equations for the polyhedral model.

Parameter name	Equation
Subtend semi-angle ψ	$n \tan\xi + m \tan\psi = 0$
Chiral angle θ	$\cos^2\theta = \frac{n^2\cos^2\psi + m^2\sin^2\psi}{n^2\cos^2\psi + m^2}$
Adjacent bond angle ϕ	$\cos\phi = (m^2\sin^2\psi)/(n^2\cos^2\psi + m^2)$
Opposite bond angle ω_1	$\cos\omega_1 = 2\cos^2\theta\sin^2\psi - 1$
Opposite bond angle ω_2	$\cos\omega_2 = \frac{2(m^2 - n^2\tan^2\theta)}{m^2 + n^2\cos^2\psi} - 1$
Nanotube radius r	$r = (\sigma\cos\theta)/(2\sin\psi)$
Perceived inner radius r_{in}	$r_{\text{in}} = r\cos\psi$
Thickness δ	$\delta = [\sigma\cos\theta\tan(\psi/2)]/2$
Number of atoms in unit cell N	$N = (n^2 + m^2)/d_R$
Unit cell length L	$L = [\sigma(n^2 + m^2)\sin\theta]/(md_R)$

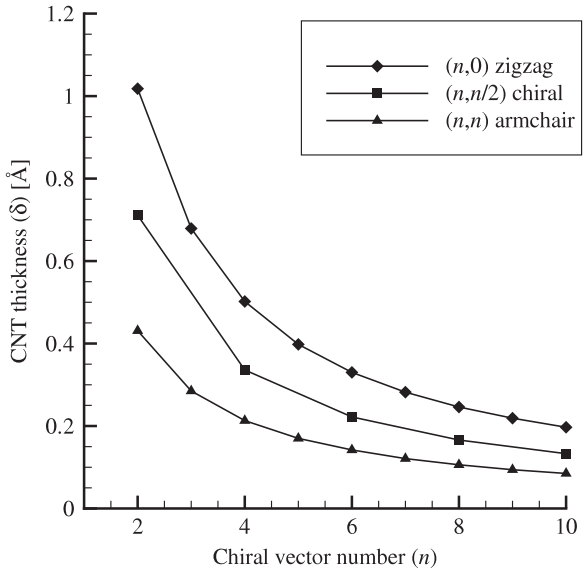

Figure 17. Thickness δ for carbon nanotubes of type zigzag: (2, 0)–(10, 0), chiral: (2, 1)–(10, 5) and armchair: (2, 2)–(10, 10).

the polyhedral model for the chiral angle (22), radius (24) and unit cell length (27) we observe that the leading order term of the analytical expressions gives the conventional formulae as their highest-order term and the second term is a first-order correction to the conventional model. This demonstrates that the polyhedral model converges to the conventional model for large n.

6. Conclusions

Silicon nanotubes may be formed from stable structures by sp^3 bond hybridization which leads to four-coordinated atoms that adopt a square lattice or a skew rhombic lattice. By employing an exact polyhedral model which is based on the three fundamental postulates that all bond lengths are equal, all bond angles are equal and all atoms are equidistant from a common axis, we have derived equations for the key geometric parameters that arise in this model, such as subtend angle 2ψ, radius r, thickness δ and unit cell length L (see table 3). The subtend semi-angle ψ is the fundamental variable on which all the other parameters depend and we find that it is determined from a transcendental equation (9) and cannot be written as a simple analytical function of n and m. We again emphasize that although we have adopted all bond lengths to be equal, a similar but more sophisticated polyhedral model could incorporate unequal bond lengths. Our approach here is first to validate the idealized model and then subsequent modifications can be viewed as deviations from the ideal model behaviour.

For ultra-small silicon nanotubes, the tube surface has a very large curvature so the tubes appear to be more like a polyhedral structure than a tubular structure; the (2, 1) and (2, 2) tubes are especially polyhedral. We also find that the (1, 0), (1, 1) and (2, 0) nanotubes do not exist with sp^3 bonded materials. Our comparison of the radii of the nanotubes with Li *et al* [2] shows that the radii predicted by the polyhedral model are in good agreement with molecular dynamics calculations. In this paper we introduce the new terminology prismatic and antiprismatic for the silicon nanotubes $(n, 0)$ and (n, n) respectively, since the corresponding terms zigzag and armchair for carbon nanotubes are entirely inappropriate in this context. Some limited numerical calculations using the LAMMPS software indicates that the smaller structures proposed here such as (5, 0), (6, 0) and (7, 0) are meta-stable, while the larger are not (i.e. (8, 0), (9, 0), etc). These findings indicate that our model applies to physically relevant structures and the results are entirely consistent with experimental outcomes since in practice, ultra-small and very large radii nanotubes tend not to occur, and there is a definite range of radii where nanotubes are experimentally observed [11, 33].

An interesting difference arising from the polyhedral model for carbon nanotubes, is that for the silicon nanotubes the chiral angle in the antiprismatic case depends on n. For silicon nanotubes, the conventional model gives the chiral angle for the antiprismatic type to be a constant 45°. However, the polyhedral model predicts that the value of the chiral angle for the antiprismatic starts from 35.26° and asymptotes to 45° in the limit of n becoming large. The adjacent bond angle ϕ in the chiral and antiprismatic types asymptotes to 90° in the limit of n becoming large. The adjacent bond angle has the constant value 90° in the prismatic type. The opposite bond angles ω_1 and ω_2 asymptote to 180° in the limit of n

becoming large, except for the prismatic type which has the constant value 180° for ω_2. The values of the opposite bond angles ω_1 and ω_2 are equal for the antiprismatic nanotubes. The other major outcome of this model is that for silicon nanotubes we may define an inner radius, and thus we may conceive a nanotube thickness which becomes thinner as the nanotube radius increases, but has a significant value for small nanotubes. The polyhedral model converges to the conventional model for large n because the leading term of the analytical expressions gives the conventional formulae as the highest-order term, while the second-order term may be viewed as a first-order correction to the conventional model. When the value of n is greater than or equal to 6, the percentage difference between the polyhedral model and the conventional model for the nanotube radius is less than 5%. For antiprismatic and chiral nanotubes, the unit cell length for polyhedral model L, is shorter than the conventional unit cell length L_0. The unit cell length for prismatic nanotubes in both models has the same value.

Acknowledgments

The support of the Australian Research Council, both through the Discovery Project Scheme and for providing an Australian Professorial Fellowship for JMH is gratefully acknowledged. We also acknowledge the help of Dr Shaun Hendy for many useful discussions and assistance with the LAMMPS software.

Appendix. Asymptotic expansions of exact formulae

The root of the subtend semi-angle ψ in (9) is determined by a series expansion in powers of $1/n$ and we then use this as the basis for determining series expansions for all of the other parameters derived in section 3. Firstly, (9) is written in the form

$$\tan\xi + h\tan\psi = 0, \tag{A.1}$$

where $\xi = (\psi - \pi/n)/h$ and $h = m/n$. The numbers m and n are assumed to be of the same magnitude, so that the order of h is assumed to be one. ψ becomes small as n increases, and therefore (A.1) can be expanded in terms of ψ and $1/n$, where we define the series as

$$\psi = \frac{\psi_0(h)}{n} + \frac{\psi_1(h)}{n^3} + \frac{\psi_2(h)}{n^5} + \cdots,$$
$$\cos^2\theta = a_0(h) + \frac{a_1(h)}{n^2} + \frac{a_2(h)}{n^4} + \cdots.$$

By the method of asymptotic expansions we may derive

$$\psi_0(h) = \frac{\pi}{1+h^2}, \qquad \psi_1(h) = -\frac{h^2\pi^3(1-h^2)}{3(1+h^2)^4}, \tag{A.2}$$

which gives ψ is in its asymptotic form (19), by substituting for $h = m/n$ in (A.2).

Now the equation for $\cos^2\theta$ (12) is expanded by substituting the asymptotic expansion for ψ. As a result, we find that the expansion coefficients are given by

$$a_0(h) = \frac{1}{1+h^2}, \qquad a_1(h) = \frac{\pi^2 h^4}{(1+h^2)^4}.$$

The adjacent bond angle ϕ is found from substituting the asymptotic equation of ψ in (13) which is given by

$$\cos\phi = \frac{h^2\pi^2}{(1+h^2)^3}\frac{1}{n^2} + \frac{h^2\pi^4(2-3h^2+2h^4)}{3(1+h^2)^6}\frac{1}{n^4} + \mathrm{O}\left(\frac{1}{n^6}\right).$$

The series expansion of the opposite bond angle ω_1 is found by substituting the series expansion for $\cos^2\theta$ and expanding the asymptotic equation for ψ. As a result, $\cos\omega_1$ is given by

$$\cos\omega_1 = -1 + 2C^2\psi^2 - (2C^2\psi^4)/3 + \mathrm{O}(\psi^6),$$

where $C = \cos\theta$. The asymptotic expansion of the opposite bond angle ω_2 is obtained by substituting the series expansions for ψ and $\cos\theta$ given by

$$\cos\omega_2 = -1 + \frac{2h^4\pi^2}{(1+h^2)^3}\frac{1}{n^2} - \frac{2h^4\pi^4(h^4+3h^2-5)}{3(1+h^2)^6}\frac{1}{n^4} + \mathrm{O}(\psi^6).$$

By substitution of the series expansion for $\cos\theta$ into the formula for the nanotube radius $(16)_1$, and then expanding as a series in powers of ψ, we derive

$$r = (\sigma C)/(2\psi) + (\sigma C\psi)/12 + \mathrm{O}(\psi^3), \tag{A.3}$$

where $C = \cos\theta$. From (17) and the series for $\tan(\psi/2)$, the thickness δ is obtained in the following form

$$\delta = (\sigma C\psi)/4 + (\sigma C\psi^3)/48 + \mathrm{O}(\psi^5). \tag{A.4}$$

The unit cell length L (18) can be expressed by the following expansion

$$L = \frac{\sigma\sqrt{1+h^2}}{d_R}n - \frac{\sigma\pi^2h^2}{2(1+h^2)^{5/2}d_R}\frac{1}{n} + \mathrm{O}\left(\frac{1}{n^3}\right). \tag{A.5}$$

From (A.3)–(A.5) and the series expansions (19) and (21) for ψ and $C = \cos\theta$, we may produce expansions for the nanotube radius r, thickness δ and unit cell length L, which are given by (23), (25) and (26), respectively.

References

[1] Iijima S 1991 *Nature* **354** 56
[2] Li B X and Cao P L 2004 *J. Mol. Struct. (Theochem.)* **679** 127
[3] Zhang L and Zhang Y 2005 *Physics (Wuli)* **34** 191
[4] Zhang M, Kan Y H, Zang Q J, Su Z M and Wang R S 2003 *Chem. Phys. Lett.* **379** 81
[5] Zhang R Q, Lee S T, Law C K, Li W K and Teo B K 2002 *Chem. Phys. Lett.* **364** 251
[6] Durgun E, Tongay S and Ciraci S 2005 *Phys. Rev.* B **72** 075420
[7] Perepichka D F and Rosei F 2006 *Small* **2** 22
[8] Wang X, Huang Z, Wang T, Tang Y W and Zeng X C 2008 *Physica* B **403** 2021
[9] Bai J, Zeng X C, Tanaka H and Zeng J Y 2004 *Proc. Natl Acad. Sci.* **101** 2664
[10] Sha J, Niu J, Ma X, Xu J, Zhang X, Yang Q and Yang D 2002 *Adv. Mater.* **14** 1219
[11] Castrucci P, Scarselli M, Crescenzi M D, Diociaiuti M, Chaudiari P S, Balasubramanian C, Bhave T M and Bhoraskar S V 2006 *Thin Solid Films* **508** 226
[12] Jeong S Y, Kim J Y, Yang H D, Yoon B N, Choi S H, Kang H K, Yang C W and Lee Y H 2003 *Adv. Mater.* **15** 1172

[13] Byun K R, Kang J W and Hwang H J 2003 *J. Korean Phys. Soc.* **42** 635
[14] Ponomarenko O, Radny M W and Smith P V 2004 *Surf. Sci.* **562** 257
[15] Dresselhaus M S, Dresselhaus G and Saito R 1992 *Phys. Rev.* B **45** 6234
[16] Dresselhaus M S, Dresselhaus G and Saito R 1995 *Carbon* **33** 883
[17] Jishi R A, Dresselhaus M S and Dresselhaus G 1993 *Phys. Rev.* B **47** 16671
[18] Yang X and Ni J 2005 *Phys. Rev.* B **72** 195426
[19] Durgun E and Ciraci S 2005 *Turk. J. Phys.* **29** 307
[20] Zhang R Q, Lee H L, Li W K and Teo B K 2005 *J. Phys. Chem.* B **109** 8605
[21] Plimpton S J 1995 *J. Comput. Phys.* **117** 1
[22] Stillinger F H and Weber T A 1985 *Phys. Rev.* B **31** 5262
[23] Cox B J and Hill J M 2007 *Carbon* **45** 1453
[24] Cox B J and Hill J M 2008 *Carbon* **46** 711
[25] Kang J W, Seo J J and Hwang H J 2002 *J. Nanosci. Nanotechnol.* **2** 687
[26] Barnard A S and Russo S P 2003 *J. Phys. Chem.* B **107** 7577
[27] Yan B, Zhou G, Wu J, Duan W and Gu B L 2006 *Phys. Rev.* B **73** 155432
[28] Zhu W, Yan X and Xiao Y 2008 *Phys. Lett.* A **372** 1308
[29] Ni M, Luo G, Lu J, Lai L, Wang L, Jing M, Song W, Gao Z, Li G, Mei W N and Yu D 2007 *Nanotechnology* **18** 505707
[30] Li B X, Cao P L, Zhang R Q and Lee S T 2002 *Phys. Rev.* B **65** 125305
[31] Dumitrica T, Hua M and Yakobson B I 2004 *Phys. Rev.* B **70** 241303(R)
[32] Durandurdu M 2006 *Phys. Status Solidi* b **243** R7
[33] Singh A K, Kumar V, Briere T M and Kawazoe Y 2002 *Nano Lett.* **2** 1243